

INFECTIOUS DISEASES

Incomplete genetic reconstitution of B cell pools contributes to prolonged immunosuppression after measles

Velislava N. Petrova^{1*}, Bevan Sawatsky², Alvin X. Han^{3,4}, Brigitta M. Laksono⁵, Lisa Walz^{2†}, Edyth Parker⁴, Kathrin Pieper⁶, Carl A. Anderson¹, Rory D. de Vries⁵, Antonio Lanzavecchia⁶, Paul Kellam^{7,8‡}, Veronika von Messling^{2‡§}, Rik L. de Swart^{5‡}, Colin A. Russell^{4‡*}

Measles is a disease caused by the highly infectious measles virus (MeV) that results in both viremia and lymphopenia. Lymphocyte counts recover shortly after the disappearance of measles-associated rash, but immunosuppression can persist for months to years after infection, resulting in increased incidence of secondary infections. Animal models and *in vitro* studies have proposed various immunological factors underlying this prolonged immune impairment, but the precise mechanisms operating in humans are unknown. Using B cell receptor (BCR) sequencing of human peripheral blood lymphocytes before and after MeV infection, we identified two immunological consequences from measles underlying immunosuppression: (i) incomplete reconstitution of the naïve B cell pool leading to immunological immaturity and (ii) compromised immune memory to previously encountered pathogens due to depletion of previously expanded B memory clones. Using a surrogate model of measles in ferrets, we investigated the clinical consequences of morbillivirus infection and demonstrated a depletion of vaccine-acquired immunity to influenza virus, leading to a compromised immune recall response and increased disease severity after secondary influenza virus challenge. Our results show that MeV infection causes changes in naïve and memory B lymphocyte diversity that persist after the resolution of clinical disease and thus contribute to compromised immunity to previous infections or vaccinations. This work highlights the importance of MeV vaccination not only for the control of measles but also for the maintenance of herd immunity to other pathogens, which can be compromised after MeV infection.

INTRODUCTION

Measles is a highly contagious infectious disease caused by measles virus (MeV). Vaccination via the measles-mumps-rubella (MMR) vaccine has been a major factor in reducing childhood morbidity and mortality, with an ~80% reduction in measles cases between 2000 and 2017 (with an estimated 21.1 million lives saved) (1). However, the rise of antivaccination campaigns and nonvaccinating religious communities, together with the limited access to the vaccine in some geographic areas, challenges the maintenance of herd immunity and leaves millions of people unprotected. Outbreaks in unvaccinated communities led to 110,000 measles deaths globally in 2017, making measles one of the leading causes of infectious disease-associated childhood mortality (2).

¹Department of Human Genetics, Wellcome Sanger Institute, Cambridge, UK. ²Veterinary Medicine Division, Paul-Ehrlich-Institut, Federal Institute for Vaccines and Biomedicines and DZIF TTU Emerging Infections, Langen, Germany. ³Bioinformatics Institute, Agency for Science, Technology and Research (A*STAR), Singapore, Singapore. ⁴Laboratory of Applied Evolutionary Biology, Department of Medical Microbiology, Academic Medical Center, University of Amsterdam, Amsterdam, Netherlands. ⁵Department of Viroscience, Postgraduate School of Molecular Medicine, Erasmus MC, University Medical Centre Rotterdam, Rotterdam, Netherlands. ⁶Institute for Research in Biomedicine, Università della Svizzera Italiana, Bellinzona, Switzerland. ⁷Department of Medicine, Division of Infectious Diseases, Imperial College Faculty of Medicine, Wright Fleming Institute, St Mary's Campus, London, UK. ⁸Kymab Ltd., The Bennet Building, Babraham Research Campus, Cambridge, UK.

*Corresponding author. Email: vp5@sanger.ac.uk (V.N.P.); c.a.russell@amc.uva.nl (C.A.R.)

†Present address: CureVac AG, Schumannstrasse 27, 60325 Frankfurt, Germany.

‡These authors contributed equally to this work.

§Present address: Life Science Division, German Federal Ministry of Education and Research, Kapelle-Ufer 1, Berlin, Germany.

MeV infection is associated with strong immune activation, generation of lifelong immunity to subsequent MeV infection, and, paradoxically, profound immunosuppression (3, 4). The immunological consequences of measles have been shown to persist up to several years after infection, leading to an increased rate of childhood mortality (5). A recent cohort study of measles in the United Kingdom showed that ~10 to 15% of children showed signs of immunosuppression 5 years after having measles, leading to increased incidence of secondary infections (6). *In vitro* and *in vivo* studies of MeV infection in macaques have suggested both direct and indirect mechanisms for MeV-induced immunosuppression including lymphopenia (7, 8), inhibition of lymphocyte proliferation (9, 10), skewing toward type 2 cytokine responses (11), and a depletion of immunological memory (12, 13). However, the exact mechanisms underlying measles-associated immunosuppression in humans remain poorly characterized.

MeV can infect B and T lymphocytes, dendritic cells, hematopoietic stem cells (HSCs), and macrophages expressing the cellular receptor CD150 (14, 15). Although the levels of total circulating lymphocytes recover by 4 weeks after infection (16), measles has been shown to result in depletion of specific B and T memory cell subsets and an increase in newly generated transitional B cells, suggesting a form of immune resetting (17). It remains unclear whether adaptive immune cells recover their complete breadth of antigen specificities to ensure efficient recognition of novel antigens and recall responses to previously encountered ones.

The ability of the adaptive immune cells to recognize different antigens is determined by the genetics of their immune receptor molecules. For B cells, the binding of the B cell receptor (BCR) variable region to an antigen leads to clonal expansion of B cells with specific BCRs and further mutations in immunoglobulin genes to

Copyright © 2019
The Authors, some
rights reserved;
exclusive licensee
American Association
for the Advancement
of Science. No claim
to original U.S.
Government Works

Downloaded from <http://immunology.sciencemag.org/> by guest on November 1, 2019

improve antigen binding affinity (18). Therefore, the degree of sequence diversity of BCR genes reflects the breadth of the BCR repertoire after antigen exposure (19). Because the immunoglobulin sequence underlies BCR specificity and antibody effector functions, we hypothesized that changes in circulating B lymphocytes after MeV infection would be reflected in the genetic composition of the immune receptor repertoire of MeV-infected individuals, particularly because naïve and memory B cells are both targets of the MeV infection. Therefore, we used isotype-resolved immune receptor sequencing (20) to monitor the BCR repertoire diversity in peripheral blood of unvaccinated children from an Orthodox Protestant community in the Netherlands sampled before and after measles [see Materials and Methods and (17) for details] to investigate the contribution of B cell impairment to measles-associated immunosuppression.

RESULTS

Dynamics of lymphocyte cell counts after measles

We characterized the genetic changes in the B naïve and B memory compartments of 26 unvaccinated children after measles (Fig. 1A and table S1). We used the sequence identity of the BCR to follow the changes of individual B cell clones in post-infection samples. To reduce the impact of background variation in immune composition over time and to distinguish MeV-specific effects from exposure to other antigens, we included two control groups: (i) unvaccinated children from the same community who did not develop measles and did not seroconvert during the study period and (ii) adults

vaccinated with a trivalent inactivated influenza vaccine (TIIV) and sampled at similar time intervals (table S2).

We first sorted naïve and memory B and T cells (sorting strategy summarized in fig. S1) and determined the changes in their relative frequencies across sampling time points (table S2). To avoid any biases introduced by differences in repertoire sampling across time points or cell-specific differences in BCR RNA expression, we ensured consistent cell counts and sequencing depth for each cohort across time points (fig. S2 and tables S2 and S3) and removed the plasmablasts ($CD19^+CD27^+CD38^+$) from B memory populations (fig. S1). Measles cases sampled >14 days after rash (20 of 26 MeV-infected individuals) did not show significant changes ($P > 0.05$) in the frequencies of lymphocyte populations ($CD19^+CD27^-$ B naïve cells, $CD19^+CD27^+$ B memory cells, $CD3^+CD45RA^+$ T naïve cells, and $CD3^+CD45RO^+$ T memory cells) across time points (Fig. 1B). Similar consistency in frequencies of sampled lymphocyte was also observed for uninfected and vaccinated controls. The consistent lymphocyte counts across sampling time points suggest that any observed changes in BCR repertoire composition result from incomplete recovery of preinfection diversity rather than differences in the number of sampled cells.

Incomplete recovery of the genetic composition of naïve BCR repertoires after measles

Having ensured similar B cell counts across time points (fig. S2A), we investigated the qualitative changes in the genetic composition of the B cell populations as reflected in the diversity of immunoglobulin heavy chain (IGH) gene sequences. Although MeV successfully infects

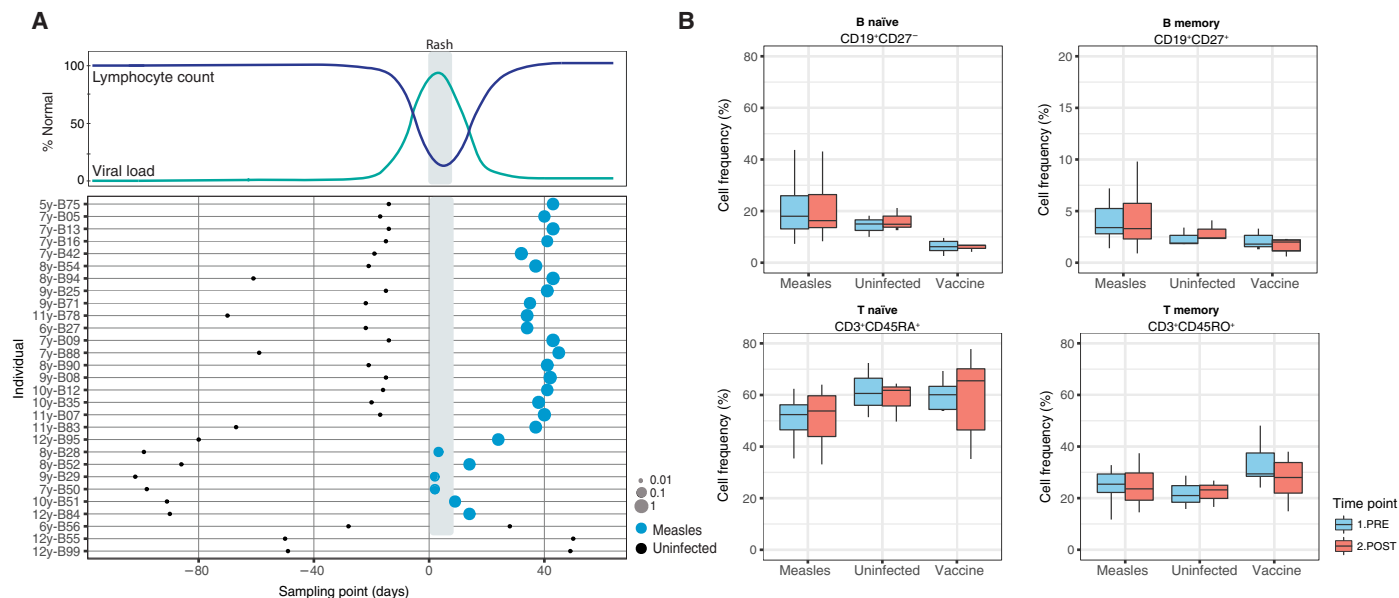


Fig. 1. Sampling strategy and lymphocyte dynamics across time points. (A) Expected timeline of MeV infection and associated lymphopenia based on disease progression in macaque model of measles (13). Sampling time points for MeV-infected cases and seronegative controls are shown relative to the onset of rash (day 0). Negative and positive values on the x axis show sampling before and after rash, respectively. The size of the dots represents the level of detected anti-MeV IgG in serum of each individual at the time of sampling (table S1). Three individuals remained seronegative (B55, B56, and B99) at both sampling points and were used as uninfected controls. Individual B56 reported rash but did not seroconvert. Sample name labels include the age of each individual followed by the unique sample identifier. (B) Frequencies (as percentages of the total sorted live PBMCs for each individual) of FACS-sorted lymphocyte populations across time points ("1.PRE": before infection; "2.POST": after infection, influenza vaccination or across the two sampling time points for the uninfected individuals). Only measles cases sampled >14 days after rash were included in the "Measles" group in (B), and the "Vaccine" group represents individuals vaccinated with TIIV. No significant changes were detected in case or control groups across time points (Wilcoxon signed-rank test with Bonferroni correction for multiple comparisons). FACS-sorted cell counts are shown in table S2. Gating strategy is shown in fig. S1.

B naïve cells, these cell populations have been shown to recover to normal frequencies after measles (17). In healthy individuals, the naïve B cell compartment is maintained via homeostatic proliferation of hemopoietic B cell progenitors in the bone marrow, which shapes the genetic diversity of the naïve BCRs (21). Therefore, we hypothesized that if the bone marrow niche is not impaired after MeV infection, the recovered naïve B cell frequencies would result in similar genetic composition as before infection. To remove any contamination of the B naïve compartment with antigen-exposed CD19⁺CD27⁻ B cells, we considered as naïve cell-derived only unmutated BCR transcripts associated with immunoglobulin M (IgM) or IgD isotypes.

Naïve B cells sampled from the same individual across time points showed high correlation of IGHV-J gene frequencies in control groups ($R^2 = 0.96$ and 0.92 in vaccinated and uninfected control groups, respectively) without significant differences in gene expression ($P > 0.05$, Wilcoxon signed-rank test) (Fig. 2A). In contrast, despite the recovery to preinfection cell frequencies, measles cases showed significant changes in IGHV-J gene frequencies ($P = 0.01$) and reduced correlation in gene expression ($R^2 = 0.78$) (Fig. 2A). The shift in IGHV-J gene frequencies was extreme in two individuals who exhibited significant change in IGHV-J frequencies [B35, $P = 1.2 \times 10^{-13}$; B42, $P = 2.4 \times 10^{-6}$; false discovery rate (FDR)-corrected Wilcoxon signed-rank test]. This marked effect on the genetic composition of the B naïve compartment was not driven by any technical biases in sorted B cell populations or BCR repertoire capture (see the Supplementary Materials). To assess whether genetic restructuring in the naïve compartment occurred in the rest of the measles cases but in a less extreme phenotype, we next followed the genetic changes in BCR repertoire at the level of clonotypes. Because the naïve compartment consists of antigen-inexperienced B cell clones that have not undergone clonal expansion, the “clonotype” definition (BCR sequences with identical IGHV and IGHJ genes and CDR3 amino acid length) used here reflects changes in the general features of the genetic composition of the naïve compartment rather than a change in the size of specific clonally related populations. In addition to individuals B35 and B42, significant changes in clonotype frequency were observed in 60% of measles cases (fig. S3) compared with 30% of vaccinated individuals and none of the uninfected controls.

Changes in naïve repertoire composition in the entire measles cohort were further evident in the significant shift to shorter CDR3 length observed across the entire measles cohort ($P = 0.0006$, Wilcoxon signed-rank test across mean CDR3 length per IGHV gene) (Fig. 2B). This effect represented a global pattern of CDR3 length distribution in the naïve repertoire and was maintained even after removal of individuals B35 and B42 ($P = 0.0004$). The skew to shorter CDR3 lengths was not observed in uninfected or vaccinated controls (Fig. 2B).

Signatures of immunological immaturity of the naïve BCR repertoires after measles

The change in IGHV-J gene frequencies in individuals B35 and B42 was driven by a loss of ~80% of IGHV genes and a shift to IGHD-proximal IGHV gene usage (Fig. 2, C and D). The previously dominant IGHV4-34 and IGHV3-23 genes were reduced ~300-fold (down to ~0.04%) in individual B35 and were completely undetectable in B42. The IGHD-proximal IGHV gene IGHV2-5 previously reported to be enriched after B cell depletion (22) was also overrepresented in individuals B35 and B42 after MeV infection, constituting 10 and

18% of the total BCR repertoire, respectively. Such a skew in IGHV gene representation was not observed in any of the other MeV-infected individuals or the influenza-vaccinated group and is unlikely to represent an antigen-driven effect (Fig. 2E).

Despite the expression of a restricted number of IGHV genes (i.e., only 30 of 300 possible IGHV-J gene combinations), the naïve repertoires of both B35 and B42 were represented by 23 different CDR3 lengths, varying between 7 and 31 amino acids (mean, 17 amino acids). This suggests that the shift in variable gene expression was not driven by an expansion of a single or limited number of naïve B cell progenitors, which would result in a clonal population of B cells with identical IGHV-D-J recombination, as observed in the context of B cell malignancies. Network analysis (23) of BCR repertoire diversity of individuals B35 and B42 compared with a patient with chronic lymphocytic leukemia (CLL) and an individual after influenza vaccination further confirmed the lack of expansion of single BCR sequences and showed high clonal diversity of the naïve B cell compartment after MeV infection [Fig. 2F, largest network cluster size: 1.1% (B35) and 0.73% (B42) compared with 89% for CLL and 2.6% for postvaccine clusters]. The high BCR nucleotide diversities in individuals B35 and B42 suggest a successful generation of new naïve B cells but with preferential use of a limited number of IGHV-J gene combinations with an overrepresentation of IGHD-proximal IGHV genes (Fig. 2, B and C).

The recognition of new antigens is dependent on the availability of a diverse pool of naïve cells. The restricted use of specific IGHV genes of the naïve BCR repertoire after measles would likely limit an individual's ability to respond to a novel antigen challenge and lead to increased susceptibility to infections, as observed in neonates (24). Similar genetic skewing in BCR recombination toward IGHD-proximal IGHV genes is a hallmark of the early stages of fetal B cell repertoire development and, together with the overrepresentation of B cells with short CDR3s, is a marker of immature BCR repertoires (25, 26). These observed signs of immunological immaturity (27) are consistent with the increase in transitional B cells after measles (17) and suggest a delayed immune reconstitution that would not be detected by looking at naïve cell counts alone.

Changes in genetic diversity and isotype composition of B memory cells after measles

The observed restructuring in the B naïve compartment after measles can explain the increased susceptibility to secondary infections after measles due to the restricted ability to generate novel B cell responses. However, the increased rate of secondary infections after MeV infection could also result from compromised immune memory to previously encountered antigens, which is masked by the generation of measles-specific B cell clones [referred to as immune amnesia (12, 13, 17, 28)]. To test the immune amnesia hypothesis, we used the genetic changes in the B cell compartment to follow the dynamics of preexisting immune memory and the generation of measles-specific response after infection.

Uninfected and vaccinated controls exhibited a stable genetic composition of B memory cells without significant changes in CDR3 lengths or mutational frequency of IGHV genes across time points ($P > 0.05$, Wilcoxon signed-rank test per IGHV gene) (Fig. 3A). By contrast, B memory cell populations after measles showed significant increases in mutational frequency ($P = 0.0008$) and a reduction in CDR3 length ($P = 0.017$) of IGHV genes, consistent with the strong immune activation caused by MeV (13).

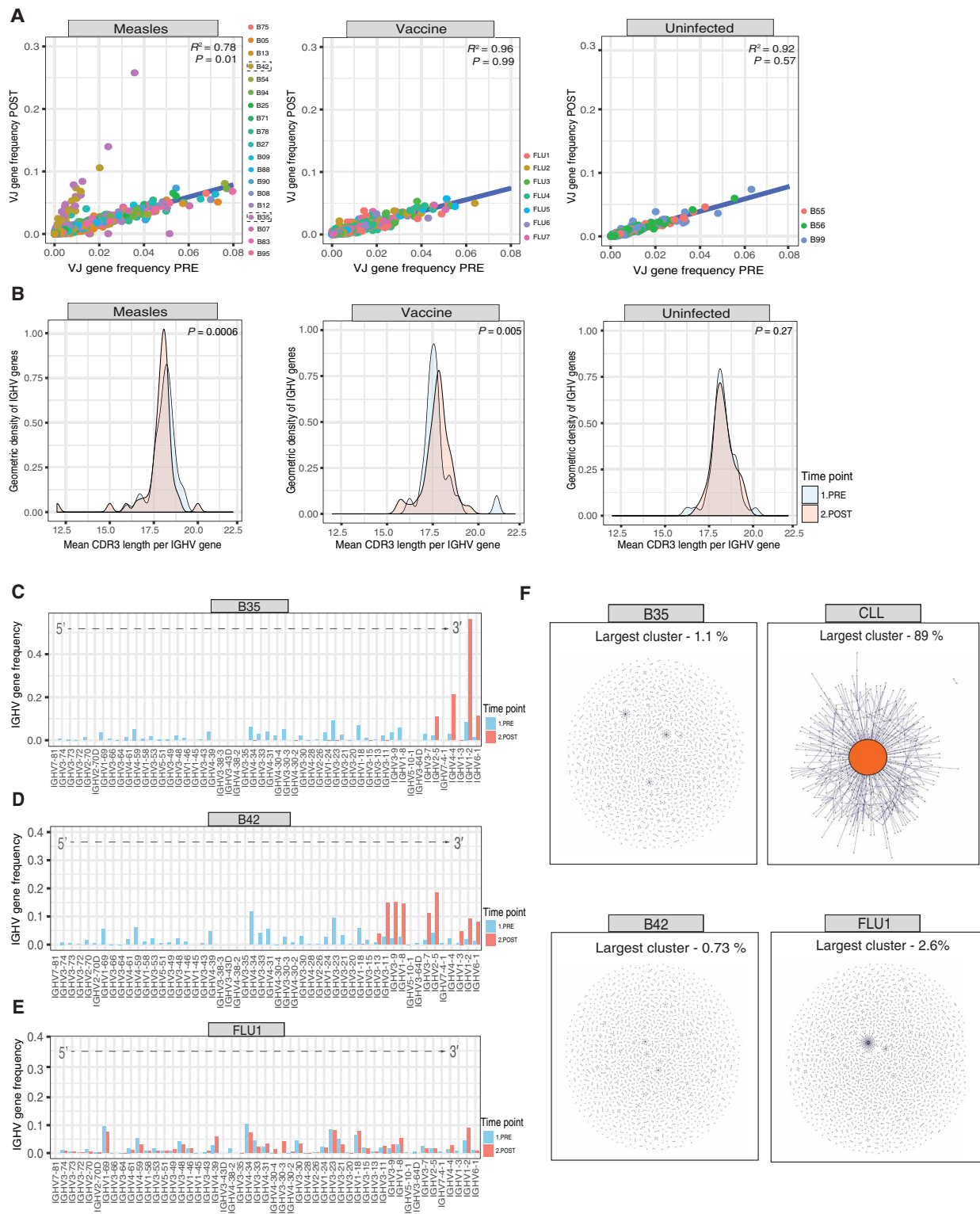
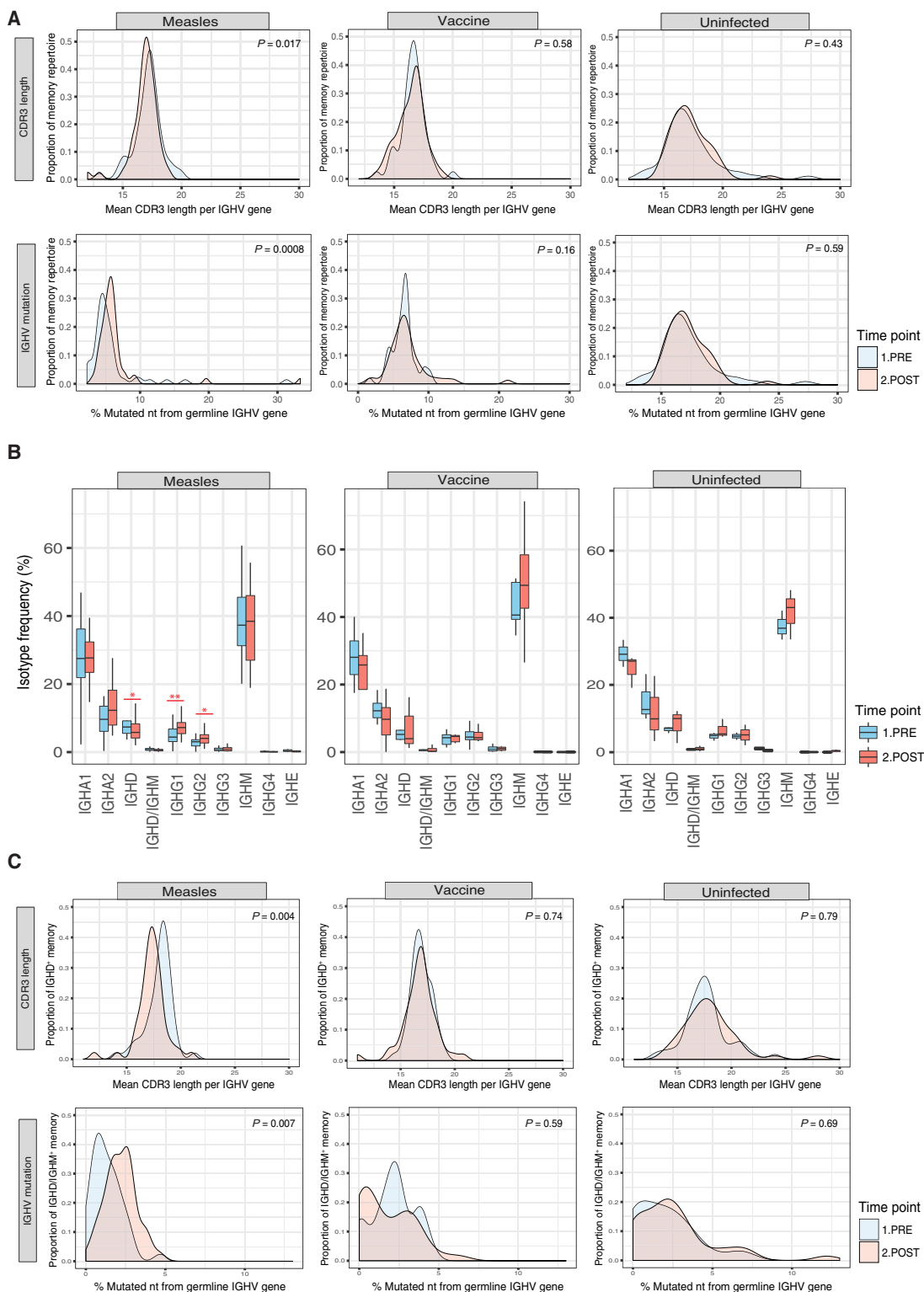


Fig. 2. Genetic changes in the B naive compartment across time points. (A) Pearson correlation of IGHV-J gene frequencies (based on total BCR reads per sample) in measles cases and vaccinated and uninfected controls colored by individuals. The P values represent the significance in differences of IGHV-J gene frequencies across time points (Wilcoxon signed-rank test). (B) Geometric density distribution of mean CDR3 lengths per IGHV gene across measles cases and vaccinated and uninfected controls. Frequencies of individual IGHV genes before and after measles for individuals B35 (C) and B42 (D) compared with individual FLU1 (E) as a representative of influenza-vaccinated individuals. The genes are ordered in a distal to proximal 5'-3' direction (left to right) relative to their location away from the IGH D gene. (F) Network properties of BCR repertoires of B35 and B42 after measles, compared with a malignant clonal expansion in an individual with CLL and a representative influenza-infected individual (FLU1). Each dot represents a unique BCR sequence. Vertices represent single-nucleotide differences between sequences.

Fig. 3. Genetic changes in the B memory compartment following measles. (A) Changes in mean CDR3 length distributions and mean somatic hypermutation per IGHV of total CD19⁺CD27⁺ B memory cell populations across measles cases and control cohorts (Wilcoxon signed-rank test). (B) Relative frequency of antibody classes in measles cases and controls based on BCR repertoire data (**P* < 0.05, ***P* < 0.01, Wilcoxon signed-rank test). (C) Changes in mean CDR3 length distributions and somatic hypermutation per IGHV gene in unswitched IgD⁺ and IgD⁺IgM⁺ B cell populations, respectively, for measles cases and control cohorts.



To study the effect of MeV infection on specific subsets of B memory cells (CD19⁺CD27⁺), we next followed the changes in genetic composition of B cells of different isotypes based on the expression of isotype-specific BCRs. Vaccinated and uninfected controls showed highly stable isotype profiles across time points without significant changes in frequency of any BCR isotype (Fig. 3B). By contrast, patients with measles exhibited a significant reduction in IGHD isotype frequency and an increase in class-switched IGHG1 and IGHG2 classes (*P* < 0.05, Wilcoxon rank-sum test). The reduction in frequency of unswitched IGHD populations was associated with reduced CDR3 lengths and increased mutational frequencies (Fig. 3C), which were not observed in vaccinated or uninfected controls. Similar patterns of IGHD⁺ B cell dynamics have been previously characterized after B cell-depleting therapy (22) and suggest a prolonged effect of measles-associated lymphopenia on the unswitched B memory compartment.

Depletion of previously expanded B memory cells after measles
The overrepresentation of IGHG1 and IGHG2 isotypes was not driven by a single clonal expansion, and IgG1 and IgG2 B cell subsets after MeV infection showed significant reductions in the size of

the most expanded BCR clones (Fig. 4A). Given the reduction in the level of clonal expansion in IgG1 and IgG2 memory cells, coupled to an increase in the overall frequency of these B cell subsets, we hypothesized that these B memory subsets experience a depletion of previously expanded B cell clones and a repopulation with new B memory cells with a lower degree of clonal expansion. We identified a significant correlation between the preinfection frequency of individual IGHV-J gene combinations and their reduction in abundance after infection with the most frequent combinations

undergoing the most marked depletion after measles (Fig. 4B). This genetic restructuring leads to significant changes in IGHV-J gene usage in IgG1, IgG2, and IgG3 populations (P values: IgG1, 9.8×10^{-4} ; IgG2, 7.52×10^{-5} ; and IgG3, 6.7×10^{-4}) and were coupled to an increase in genetic diversity of these subsets (Fig. 3C). Similar increases in diversity of the B memory repertoire were also observed in the IgA2 compartment likely corresponding to repopulation of B cells at mucosal sites, where these subsets are most commonly found (29).

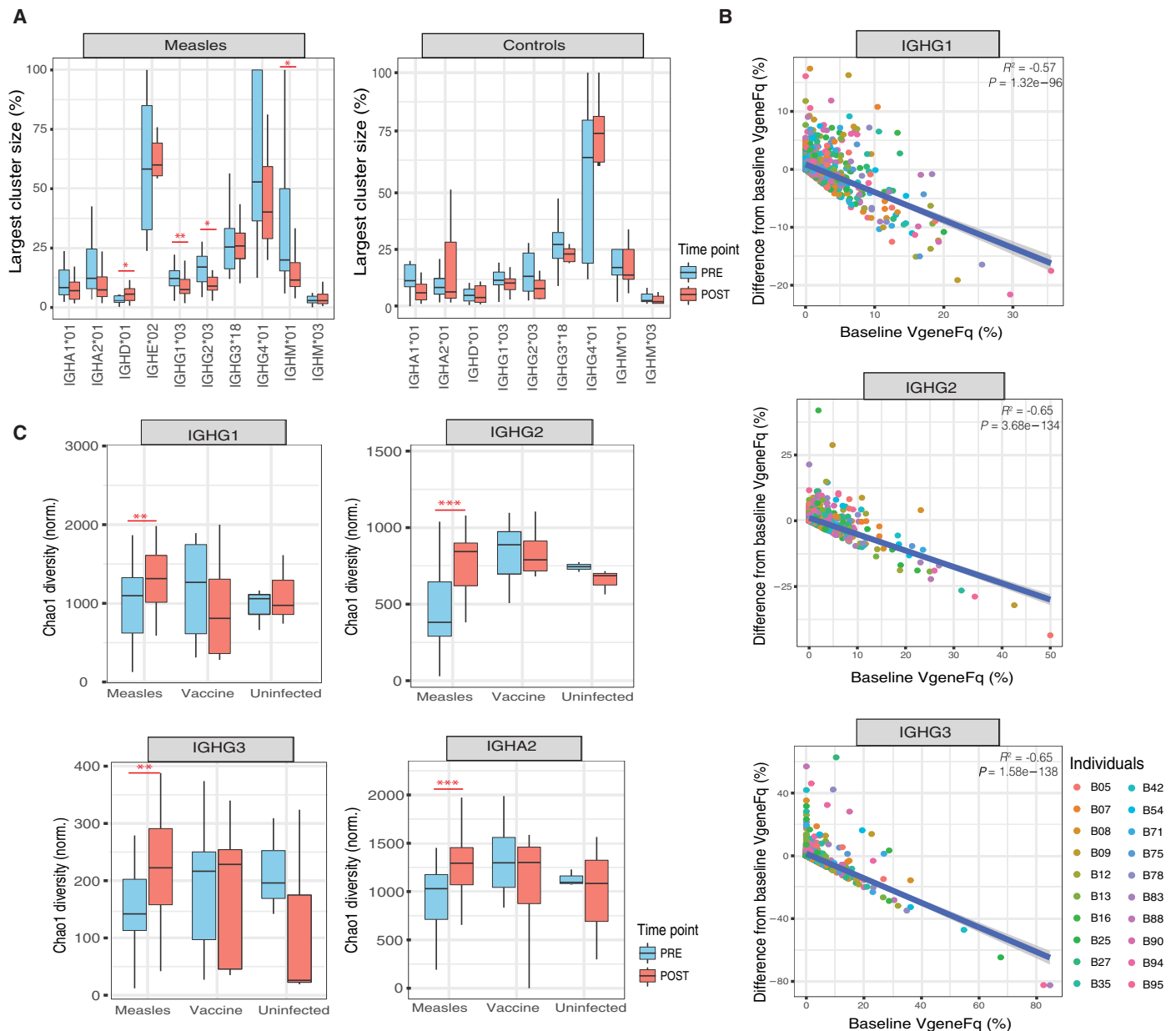


Fig. 4. Changes in clonal expansion and BCR diversity in the B memory compartment following measles. (A) Changes in B cell cluster size across isotype-specific B memory populations. B cell clusters were defined for each isotype using network analysis (see Materials and Methods). The largest cluster for each isotype was identified as the cluster constituting the highest number of BCRs. The size of the largest cluster represents the number of BCRs in this cluster as a percentage of the total BCR reads associated with the same isotype. Significance was determined using Wilcoxon rank-sum test: * $P < 0.05$, ** $P < 0.01$. (B) Relationship between IGHV gene frequency at baseline (before MeV infection) and the change in frequency after infection across IgG B memory subsets in measles cases. (C) Genetic diversity across B memory subsets measured by the chaoE diversity index (** $P < 0.01$, *** $P < 0.001$, Wilcoxon rank-sum test).

The reduction in frequency of previously expanded B cell populations, together with the changes in IGHV-J composition and increase in diversity of switched B memory subsets, suggests a remodeling of the B memory pools after measles and a depletion of highly clonally expanded IgG⁺ populations, which are not reconstituted after MeV infection. The observed persistent changes in the mutational status and IGHV gene usage of IgG⁺ B memory populations in patients after measles are consistent with the delayed reconstitution of the IgG memory compartment previously reported to occur up to 6 years after B cell–depleting therapy with rituximab (30, 31), suggesting a possible similar consequence for MeV-associated lymphopenia. The measles-associated changes in isotype-specific B memory populations were not observed in the uninfected or influenza-vaccinated controls (Fig. 4C) and thus are unlikely to represent background variation in B memory cell diversity or generation of an antigen-specific response.

Depletion of antigen-specific B cell clones in measles cases and evolution of measles-specific response

To test how MeV-induced restructuring of the B memory compartment affects the frequency of antigen-specific B cells present before infection, we followed the change in relative frequency of B cell clones with identical specificity. There is no generally agreed-upon level of CDR3 sequence identity required to infer clonal relationships from BCR data, and similarity thresholds <100% do not guarantee true clonal relatedness of the respective B cells and recognition of an identical antigen. Therefore, we used the most conservative definition of clonally related sequences (BCRs with the same IGHV, IGHD, IGJ gene annotation, and identical CDR3 amino acid sequence) to ensure stratification of the BCR repertoires into groups of sequences with identical antigen specificity. We refer to these BCR groups as B cell “clones.”

Uninfected and vaccinated controls maintained highly correlated frequencies of BCR clones across time points ($R^2 = 0.76$, $P = 0.006$), consistent with a lack of substantial BCR genetic restructuring (Fig. 5A). By contrast, patients with measles exhibited lower clonotype overlap across time points compared with control cohorts (median, 21 clonotypes for patients with MeV compared with 53 for controls) and nonsignificant correlation in frequency of shared clonotypes ($R^2 = 0.36$, $P = 0.118$) (Fig. 5B). The majority of measles cases experienced a reduction in relative abundance of clones present before infection, consistent with the immune amnesia hypothesis (12) and functional loss of previous immunity.

Because the recognition of MeV by the immune system is mediated via conformational epitopes (32), there is not a reliable recombinant protein probe for sorting of MeV-specific B cells to enable the direct quantification of antigen-specific B cell populations. However, the successful generation of measles-specific immune responses was evident from the detection of IgM and IgG MeV-specific antibodies in serum of the infected patients (table S1), demonstrating the generation of functional antigen-secreting plasma cell populations (17). The evolution of MeV-specific immune responses, together with the reduced frequency of preexisting B memory clones, suggests a restructuring in the B cell compartment, where the depletion of B memory clones is masked by the evolution of MeV-specific response. This lymphocyte dynamic resolves the lymphopenic state but does not necessarily lead to reconstitution of the preinfection immune diversity.

Clinical consequences of measles-induced B cell impairment

To investigate whether the clinical consequences of the observed changes in B cell genetic diversity, we tested the effect of morbillivirus

challenge on vaccine-induced immunity to influenza virus in ferrets infected with canine distemper virus (CDV). CDV is closely related to MeV and can be used as a surrogate model for MeV infection with associated virus-induced lymphopenia (33). Two groups of four ferrets were first vaccinated with live-attenuated influenza vaccine (LAIV) and followed over a period of 4 weeks to allow for development of immunity to influenza vaccine antigens (Fig. 6A). At 4 weeks after vaccination, one of the groups was subjected to challenge with a nectin-4–blind CDV, which retains the immunosuppressive characteristics of a lethal wild-type virus but no longer causes clinical disease (34). The CDV uninfected group maintained high levels of influenza-specific neutralizing antibodies 14 weeks after vaccination. By contrast, CDV infection led to a depletion of serological memory and a significant reduction in the titers of influenza-neutralizing antibodies compared with unchallenged and unvaccinated controls (LAIV + CDV group, Fig. 6A). Because the typical antibody half-life in ferrets is 1 to 4 days (35), the maintenance of high level of influenza-neutralizing antibodies is reliant on antibody-producing plasma cells. This B cell population appears to be successfully generated after influenza vaccination (LAIV group, Fig. 6A) but impaired after CDV challenge, leading to depletion of neutralizing antibodies (LAIV + CDV group, Fig. 6A).

In addition to the compromised serological memory, and despite the resolution of lymphopenia (Fig. 6B), CDV-infected animals exhibited impaired B memory recall responses characterized by an inability to generate influenza-neutralizing antibodies after influenza H1N1 virus challenge. The compromised immune recall response leads to higher virus titer (Fig. 6C) and increased severity of clinical symptoms 4 days after infection (Fig. 6D). The depleted protective antibody titers and the limited capacity for B memory recall in the ferret model suggest that the observed immune restructuring after morbillivirus infections results in a compromised preexisting immune state, which could contribute to increased severity of secondary infections. Such a clinical consequence of measles can explain the observed increase in the rate of secondary infections after measles due to the loss of immune protection (5).

DISCUSSION

The majority of measles-associated deaths and clinical complications are due to secondary infections that occur as a result of immunosuppression (36, 37). This clinical consequence of measles can be detected on a population level even in developed countries where there is a significant link between measles incidence and total burden of infectious disease mortality (5, 6). Despite the substantial clinical impact of measles, the immunological underpinnings of measles immunosuppression remain incompletely understood.

Various *in vitro* models have suggested suppression of lymphocyte proliferation and altered cytokine response as possible mechanisms contributing to measles-associated immunosuppression (9–11, 38, 39). However, these observations are not consistent with *in vivo* macaque models and naturally infected individuals where measles results in successful activation and marked expansion of MeV-specific lymphocytes, followed by resolution of viremia and lymphopenia (4, 13). Quantitative characterization of lymphocyte populations in infected individuals shows a reduction in specific B and T memory cell subsets coupled to increase in transitional B cells (17). However, quantifying cell populations based on fluorescence-activated cell sorting (FACS) analysis makes it difficult to identify the loss of specific B memory

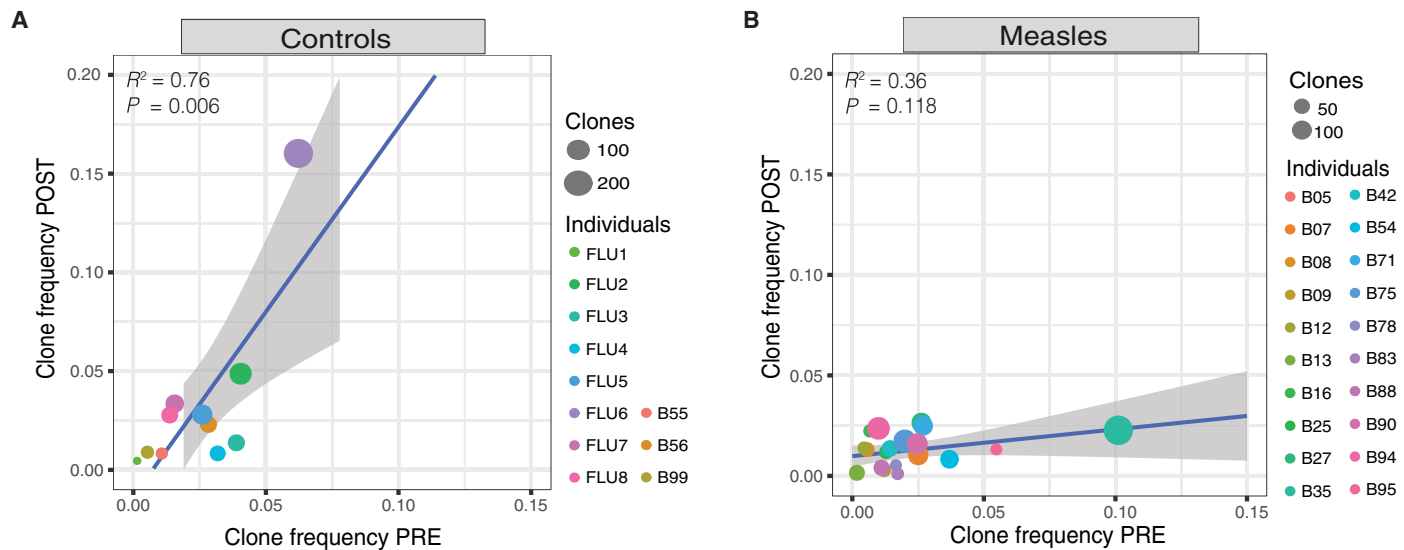


Fig. 5. Changes in frequency of antigen-specific B cell clones after measles. Pre/post-changes in relative frequency of B cell clones in uninfected and vaccinated controls (A) and in measles cases (B). Clones were defined as BCR sequences with identical V, D, and J annotation and identical CDR3 amino acid sequence. Each dot represents an individual from the respective cohort. Dot size represents the number of B cell clones shared across time points. Gray shading shows 95% confidence intervals.

clones present before infection and the repopulation of B cell subsets with novel B cell clones.

Therefore, we used the genetic sequence of the BCRs as a barcode unique for each cell, which can be tracked before and after infection to distinguish between previously available and recently repopulated B and T cell memory pools. Immunoglobulin sequencing has been previously demonstrated as a reliable tool for characterization of B cell populations of different (sub)classes (20). Using this isotype-resolved sequencing approach, we identified long-term genetic restructuring in the B naïve and B memory compartments that would be undetectable using traditional FACS-based phenotyping and absent in the uninfected and vaccinated control cohorts of our study. Our results demonstrate two modes of immune restructuring after MeV infection: (i) an incomplete bone marrow reconstitution of naïve B cell diversity leading to immunological immaturity despite resolution of clinical symptoms and (ii) a depletion of previously generated immune memory, which is maintained beyond the period of lymphopenia and can be masked by the immune activation after measles.

Under normal physiological conditions, the B cell naïve compartment is continuously repopulated with bone marrow-derived B cells via a negative feedback loop mechanism of regulation by mature B cells (40). This ensures a highly stable pool of naïve B cells with a broad range of potential antigen specificities encoded in the diversity of the recombined BCR genes. The severe contraction of immune diversity in the naïve compartment in ~10% of our measles-infected cohort and the shift to immunological immaturity of their BCR repertoires suggest a compromised bone marrow reconstitution of B cell diversity. Similar effects on the B cell homeostasis have been previously described in nonobese diabetic/severe combined immunodeficient (NOD/SCID) $IL-2R\gamma_c^{-/-}$ mice, where MeV infection of HSCs impairs the short-term ability to reconstitute the B cell compartment (41). There is no evidence that these observations are technical artifacts (see the Supplementary Materials), and the proportion of cases exhibiting this extreme phenotype is consistent with the reported frequency of secondary infections in the minority of measles cases (6). It is expected that the notable naïve compart-

ment restriction in these individuals does not occur in all infected individuals, because such high prevalence would result in substantially higher incidence of post-measles complications than currently reported. However, if the ~10% frequency observed in our study is representative of the global frequency, then the true extent of the public health consequences of measles is likely to still be underestimated. Further studies of the immune consequences of MeV infection in measles-endemic areas, particularly those that experience higher infectious disease burden than the Netherlands and the United Kingdom (6), are urgently needed.

According to the macaque model of measles, MeV replicates successfully in bone marrow of infected animals, likely affecting plasma cells and hemopoietic stem cells (13, 15). In vitro MeV infection is successfully established in both $CD34^+ CD150^-$ and $CD34^+ CD150^+$ hematopoietic stem and progenitor cell subsets, and virus can be transmitted between stem cells and stromal cells or through infected mature B and T cells (41). The ability to exchange virus between different cell types populating the bone marrow niche suggests that the bone marrow is a possible environment for sustained virus replication. The infection and loss of hemopoietic stem cells responsible for the repopulation of B naïve pools is thus a possible reason for the observed impairment of naïve B cell diversity. Depending on the developmental stage of affected progenitor cells, this would lead to either delayed reconstitution of the breadth of the naïve compartment or permanent gaps in HSC population, leading to limited response to novel antigens. Although it could not be demonstrated directly in this study, a similar form of immune impairment could underlie increased susceptibility to respiratory pathogens after measles and the development of pneumonia as the most common consequence of measles (42). This previously unrecognized immunological consequence of measles on B cell homeostasis could also explain the beneficial effect of vitamin A therapy to prevent measles complications (43) by promoting the regenerative potential of hemopoietic stem cells (44).

Although the naïve B cell pools are maintained from bone marrow progenitors, the generation of immunological memory occurs in

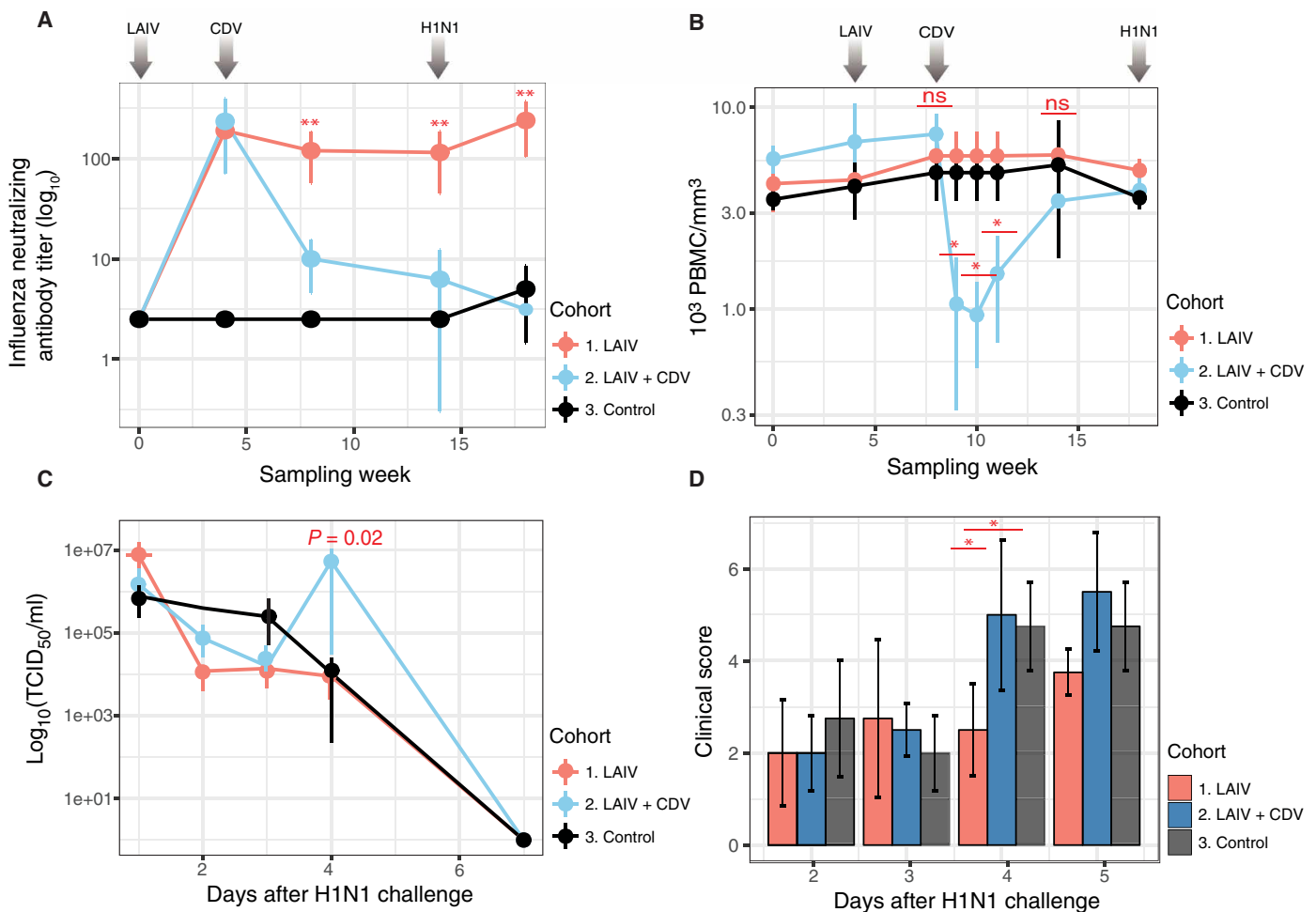


Fig. 6. Effect of lymphotropic morbillivirus challenge on vaccine-acquired immunity in a ferret model of measles. (A) Influenza-neutralizing antibody titers of ferrets after vaccination with LAIV vaccine, challenge with nectin-4–blind CDV, and live influenza virus challenge. Animals not subject to vaccination and CDV infection were used as a “Control” group. Significance of the differences in neutralizing antibody titer was determined using Wilcoxon rank-sum test: $***P < 0.01$. **(B)** Changes in lymphocyte counts of ferrets after vaccination with LAIV with or without an infection with CDV. Significance of the difference in lymphocyte counts across cohorts was determined using Wilcoxon rank-sum test: $*P < 0.05$, “ns” $P > 0.05$. **(C)** Titers of influenza H1N1 virus in nasal swabs of animals after intranasal challenge with H1N1pdm09 at week 18 (10 weeks after CDV challenge). Significance of the difference in virus titers was determined using Wilcoxon rank-sum test. **(D)** Severity of ferret clinical symptoms, based on a combined clinical score of body weight and temperature (see Materials and Methods), after influenza virus challenge. Significance of the difference in clinical score was determined using Wilcoxon rank-sum test: $*P < 0.05$.

response to antigen stimulation and, for B cells, is mediated through the BCR, which drives clonal expansion and generation of memory B cells and plasma cells (18, 45). Memory B cells carrying BCR with high affinity to previously exposed antigens mediate secondary immune responses upon rechallenge, whereas plasma cells are the main source of serological immunity and are maintained as terminally differentiated cells in the spleen and bone marrow. By following the dynamics of different subclasses of B cells after measles, we demonstrate a compromise of immunological memory through the depletion of previously expanded B cell clones and incomplete genetic reconstitution of both switched and unswitched B memory subsets. The reconstituted immune memory pools after measles show an increase in genetic diversity, likely resulting from immune activation and repopulation of B memory pools with new B cell clones. Such B cell repopulation is consistent with the observed increase in transitional B cells in measles-infected individuals (17). The increase in diversity of IgG subsets could also be explained by

repopulation of B memory pools with short-lived class-switched IgG with likely polyreactivity, as previously described (46).

It is difficult to determine the relative contribution of B cell depletion to B cell repopulation in the observed change in relative frequency of clones present before measles. However, B memory cells are the main cell type subject to MeV infection (15), and significant depletion of B memory cells after measles in the same cohort has been previously described by analyzing cell surface markers (17). Therefore, we do not expect that the reduction in relative abundance of clones present before infection to be simply a result of repopulation of B memory pools with newly expanded clones. Because the B cell population in the blood cannot grow indefinitely, the fact that the relative frequency of previously generated immune memory is reduced in peripheral blood would mean that upon re-exposure to an antigen, the probability of encounter of a specific B memory cell and efficient generation of a recall response will be lower even if not all previously generated B memory clones are lost.

In addition to the role of depleted immune memory cells in recall responses, the long-term maintenance of plasma cell pools to a specific antigen is dependent on the continuous reactivation of B memory subsets to the same antigen and their migration to the bone marrow (47). Therefore, the depletion of B memory populations would not only limit the ability to generate a recall response to previously encountered antigens but also likely impair the ability to maintain plasma cell pools able to provide serological immunity.

The direct clinical consequences of the observed B cell genetic restructuring are difficult to ascertain in the studied cohort due to the unavailability of samples from the studied subjects at later time points. Such samples are extremely difficult to collect, given the age of the children and the specific religious beliefs of the community. However, the animal model of measles demonstrates directly the depletion of serological immunity, the impaired recall response to a previously encountered antigen, and the increased severity of secondary infection, suggesting a loss of vaccine-acquired immunity as a clinical consequence of measles. The observed consequences of measles in the human cohort and in the ferret model are consistent with the clinical picture of patients after B cell-depleting therapy with the anti-CD20 antibody rituximab. The specificity of rituximab to CD20-expressing B cells enables the distinction of clinical symptoms driven specifically by B cell impairment. Patients treated with rituximab exhibit a delayed repopulation of B memory subsets several years after therapy (30, 48) and an inability to generate protective serological response to follow-up vaccination (49, 50). This impaired immunoglobulin response to vaccination is specific to B cell depletion and is not observed in other types of generalized immunosuppression (51), demonstrating that the impairment of B cell compartment alone is sufficient to compromise the protective immunity and recall responses to previously encountered antigens.

Our findings provide a biological explanation for the observed increase in childhood mortality (5) and secondary infections several years after an episode of measles (6). In addition to the direct demonstration of the previously hypothesized immunological amnesia, the consequences of measles on naïve B cell homeostasis observed here can act as a foundation for future research on the bone marrow effects of MeV infection. The depleted B memory pools and serological immunity highlights the importance of MeV vaccination not only to protect against measles but also for the maintenance of immunity to a range of other pathogens, which can be compromised after MeV infection. Given the recent record-high cases of measles, this work encourages the closer follow-up of patients with recent episodes of measles, expansion of measles vaccination campaigns, and monitoring of herd immunity to different pathogens in countries experiencing measles outbreaks.

MATERIALS AND METHODS

Study design

The main objective of the study was to study the immunological underpinnings of measles-associated immunosuppression. We monitored the changes in genetic composition of the B cell compartment after measles as a way to characterize the effects of measles on pre-existing immunity and on the ability of the immune system to maintain B cell homeostasis. The measles study cohort included unvaccinated children aged 4 to 17 years old without a history of natural measles. The participants were from three Orthodox Protestant schools in the Netherlands with vaccination coverage of <20% [for more details, see

(17)]. The seronegative and vaccinated subjects were collected to be used as control groups in this study. Blood sample collection was done after verbal assent from participants younger than 12 years old or written informed consent from participants aged 12 years and older. The parents of the study participants consulted an investigator and a research nurse but still refused all vaccinations due to religious reasons. The exclusion criteria were chronic disease and immunosuppression due to medication. None of the study participants required hospitalization due to severe measles. The study protocol was approved by the medical ethical committee of Erasmus MC, the Netherlands [MEC-2013-302, Centrale Commissie Mensbonden Onderzoek (CCMO) register NL45323.078.13/2]. Collection of peripheral blood mononuclear cell (PBMC) samples from vaccinated adult volunteers was approved under approval number MEC-2015-095. Sequencing of the samples was approved by Sanger Institute Ethics Committee under Research Ethics Committee approval numbers 14/081 and 18/034 for the Orthodox Protestant community cohort and the vaccinated adult group, respectively.

The selection of sampling time points in the measles cohort was done on the basis of symptoms of ongoing measles disease so that the first sample is before any symptoms of measles and the second is ~40 days after rash, which is expected to be beyond the period of lymphopenia. The children that remained seronegative and the adult influenza vaccine controls were sampled at similar intervals to the measles cohort (despite the lack of measles) for consistency.

FACS of the PBMC samples and allocation of sequencing lanes were performed randomly without the stratification of the case and control cohorts. The operator was blinded to the case or control status of the samples. Stratification of cases and controls was performed at the stage of data analysis to assess the results. Because of the limited availability of PBMC samples from the children cohort and the high cost of the sequencing experiments, replication of FACS and BCR sequencing was not performed. Because of poor polymerase chain reaction amplification of the RNA from the naïve compartment of the B16 pre-measles sample, the pre- and post-measles naïve compartment samples from this individual were removed. Because this is the first study of BCR genetic diversity in the context of measles, it was difficult to determine sufficient sample size and to perform power calculations. However, to ensure that we are observing measles-specific effects rather than background genetic variation, we present all results as a comparison with uninfected and vaccinated control cohorts.

Human blood samples

Twenty-six children sampled before and after laboratory-confirmed measles and 3 children sampled across two time points who remained seronegative were used as measles disease and control groups, respectively. Sampling time points and measles seroconversion titers are provided in table S1. PBMC samples from seven adults sampled before and 40 days after vaccination with TIIV were used as vaccine controls. PBMCs were isolated from heparinized blood (from the children and adult cohorts) using Ficoll density centrifugation and were frozen at -135°C in RPMI 1640 medium supplemented with 20% fetal bovine serum (FBS) and 10% dimethyl sulfoxide (DMSO).

FACS of lymphocyte populations

Frozen PBMCs were thawed in 7 ml of R10/deoxyribonuclease (DNase) solution containing RPMI 1640 media, 10% FBS, and 10 μl of DNase I (10,000 U/ml, Sigma) per 500 ml, pelleted at 2000 rpm for 5 min at 4°C , and washed in 4 ml of phosphate-buffered saline

(PBS) twice to remove residual DMSO. After the second washing step, supernatant was removed and cells were incubated with antibody staining mix (see below) for 20 min. 4',6-Diamidino-2-phenylindole (DAPI) stain was added to each sample immediately before sorting. Antibody staining mix contained the following antibodies: fluorescein isothiocyanate (FITC)-CD19 (catalog no. 555412, BD Biosciences), PeCy7-CD3 (catalog no. 557749, BD Biosciences), phycoerythrin (PE)-CD45RA (catalog no. 555489, BD Biosciences), AF700-CD45RO (catalog no. 561136, BD Biosciences), allophycocyanin (APC)-CD27 (catalog no. 558664, BD Biosciences), BV711-CD38 (catalog no. 563965, BD Biosciences), and CYTO-COMP beads (catalog no. 6607023, Beckman Coulter). Samples were sorted using BD Influx machine into five cell populations: CD19⁺CD27⁻ (B naïve cells), CD19⁺CD27⁺ (B memory cells), CD19⁺CD27⁺CD38⁺ (plasmablasts), CD3⁺CD45RA⁺ (T naïve cells), and CD3⁺CD45RO⁺ (T memory cells). Plasmablasts were derived only from the individuals sampled <14 days after rash and were not used for the analyses in this study. Raw counts of the FACS-sorted cell populations for each sample are provided in table S2. RNA from sorted B cell populations was used for amplification of IGH gene using the isotype-resolved BCR sequencing protocol described below.

Library preparation for isotype-resolved sequencing

RNA extraction was performed using RNeasy Mini Kit (Qiagen) according to the manufacturer's protocol. Library preparation for isotype-resolved BCR sequencing was performed as previously described (20). In brief, reverse transcription (RT) was run as a 20- μ l reaction with SuperScript III (Thermo Fisher Scientific). Reagents for each RT step were divided in two mixes: Mix 1 [RNA template, five IGHC region reverse primers labeled as "IGHA," "IGHM," "IGHD," "IGHE," and "IGHE" (10 μ M each reverse primer)] was incubated for 1 min at 70°C and then immediately transferred on ice for 1 min. Mix 2 [4 μ l of 5 \times FS buffer, 1 μ l of dithiothreitol (0.1 M), 1 μ l of dNTP (10 mM), and 1 μ l of Superscript III] was added and incubated at 50°C for 60 min, followed by inactivation at 70°C for 15 min. Complementary DNA (cDNA) was cleaned up with Agencourt AMPure XP beads. Cleaned cDNA was amplified with non-barcoded V-gene multiplex primer mix ("VH1- to VH6-FR1" primers) (10 μ M each forward primer) and "3' universal" reverse primer (10 μ M) using KAPA protocol. Thermal cycling conditions were as follows: one step (95°C, 5 min), 5 cycles (98°C, 5 s; 72°C, 2 min), 5 cycles (65°C, 10 s; 72°C, 2 min), 25 cycles (98°C, 20 s; 60°C, 1 min; 72°C, 2 min), and one step (72°C, 10 min). Nucleotide sequences of all used primers described above are provided in table S4.

Sequencing and barcode filtering

MiSeq libraries were sequenced using standard Illumina 300-base pair (bp) paired-ended MiSeq protocols. Processing of BCR sequencing data and correction of technical errors via barcode filtering were performed as previously described (20). In brief, MiSeq forward and reverse reads with Phred score > 34 were merged on the basis of an overlapping sequence of >50 bp. Immunoglobulin isotype identity of each read was identified after alignment to the reference constant region genes from the International Immunogenetics Information System (IMGT) database (<http://www.imgt.org>). The reads were divided in bins on the basis of the barcoded region within each reverse constant region primer. Only bins consisting of sequences with >80% sequence certainty were retained. All sequences were examined for intact open reading frame and significant similarity to

reference IGHV and IGHJ genes from the IMGT using BLAST. Scripts for all analyses described above are available from <https://github.com/VelislavaNPetrova/measlespaper/>.

Changes in lymphocyte frequencies across time points

Frequencies of sorted B and T cell populations were determined as percentage of cells from each population from the total sorted live cells per sample. Differences in lymphocyte frequencies for each cohort were determined by comparing the frequencies for each individual from the respective cohort across time points. Significance was determined using Wilcoxon rank-sum test comparing the distributions of lymphocyte frequencies of individuals from each cohort across time points. Significance threshold was determined using an α value of 0.05 and Bonferroni correction for multiple testing within each cohort.

Changes in IGHV-J gene and clonotype frequencies for each individual across time points

Frequencies of IGHV-J gene combinations were calculated as a percentage of the total repertoire (total BCR sequences) for each individual. The derived frequencies were then compared using two-sided nonparametric Wilcoxon signed-rank test, which does not assume that data in each category are normally distributed. The test is based on three assumptions: (i) the dependent variable is measured in a continuous level (which is the case for IGHV-J gene and clonotype frequencies); (ii) the categorical variable consists of matched pairs (which is the case in this dataset as the same individuals were sampled across two time points); and (iii) the distribution of differences between the two related groups is symmetrical (this is ensured by the representation of IGHV-J gene frequencies as percentage). Significance values were corrected for multiple testing using FDR correction, and significance was determined as $P < 0.05$. The same statistical method was also used to compare the changes in clonotype frequencies for each individual. Clonotypes were defined as BCRs with identical IGHV and IGHJ annotation and CDR3 length.

Network analysis

Networks representing BCR diversity in Fig. 2E were derived from network analysis as previously described (23). Briefly, each vertex represents a unique sequence in which relative vertex size is proportional to the number of identical sequence reads after barcode correction. Edges are generated between vertices that differ by single-nucleotide, non-indel differences. Clusters are collections of related, connected vertices. The largest cluster was determined as the cluster constituting the largest proportion of the BCR repertoire (in terms of number of BCR sequences).

Changes in CDR3 length distribution and mutational frequency per IGHV gene

Changes in CDR3 length distribution and mutational frequency across time points were determined for the B naïve and B memory compartments by comparing the mean CDR3 amino acid length or mean mutation from germline [using IMGT (52) annotation] per IGHV gene across time points. The total number of BCR reads of a given IGHV gene was used for each comparison. Significance was determined using paired Wilcoxon signed-rank test. Significance threshold was determined using an α value of 0.05 and Bonferroni correction for the number of IGHV genes used for the pairwise comparisons.

Frequencies and largest cluster size of isotype-specific B memory populations

Frequencies of isotype-specific B memory cell populations were determined as the percentage of total BCR reads from an individual that are associated with a given isotype (i.e., contain a given IGHC sequence). The size of the largest cluster for each isotype-specific population was estimated after performing network analysis of each isotype-specific B memory cell population per individual and determining what proportion of the total isotype-specific BCR repertoire (as BCR reads) is distributed within the largest network cluster.

Genetic properties of isotype-specific BCR repertoires

Genetic properties of isotype-specific BCR repertoires were determined on the basis of CDR3 length, mutation in IGHV gene, total IGHV-J gene frequencies, and extrapolated Chao diversity index, calculated for each isotype (sub)class. The total number of BCR sequences in the B memory compartment for each individual was first divided by isotype, depending on the detected IGHC gene. For each B memory cell subclass, we determined the changes in mean CDR3 amino acid length and mutational frequency per IGHV gene as previously described. The changes in IGHV-J gene usage per each isotype were determined as previously described. Extrapolated chao ("chaoE") diversity index per isotype was determined for each individual using VDJtools software (53) and compared across time points using paired Wilcoxon signed-rank test. IGHV-J gene frequencies were determined as percentage of each IGHV-J gene combination from the total isotype-specific repertoire across individuals and compared across time points using paired Wilcoxon signed-rank test.

B memory cell clonal overlap across time points

B memory clones were defined as BCR sequences of any isotype with identical IGHV, IGHC, and CDR3 amino acid sequence. Clonal overlap across time points was calculated for each individual using VDJtools software (53). The frequency of overlapping clones in each time point was calculated as the percentage of the clones from the total B memory cell repertoire (total number of BCR sequences) per individual.

Ferret model of immunosuppression

Influenza vaccinations and infection with CDV

Eight male ferrets (*Mustela putorius furo*) aged 16 weeks or older were vaccinated with tetravalent seasonal LAIV (Fluenz Tetra, AstraZeneca) containing an H1N1 A/INDRE/Mexico/4487/2009-like antigen by intranasal administration. All animal studies were approved by the Institutional Animal Care Committee according to German and European regulations. One group of four male ferrets was not vaccinated. Four weeks after immunization, four ferrets from the live-attenuated vaccine group were infected intranasally with 2×10^5 TCID₅₀ (median tissue culture infectious dose) of recombinant nectin-4-blind CDV derived from the 5804PeH CDV strain (33). This virus does not recognize the morbillivirus epithelial receptor nectin-4 (nectin-4-blind), thereby preventing a lethal viral infection in mice. Ten weeks after the CDV nectin-4-blind infection, all the animals from each treatment condition were infected intranasally with 5×10^5 TCID₅₀ of the virulent 2009 pandemic H1N1 influenza virus strain A/INDRE/Mexico/4487/2009 (Mx10) (54).

Blood sampling

Whole blood was collected from ferrets under general anesthesia in two lithium heparin tubes per animal. Total leukocyte counts were obtained by counting cells after mixing whole blood (10 μ l) with 3%

acetic acid (990 μ l). Heparinized blood was centrifuged for 3000 rpm for 15 min to collect plasma, and the remaining cells were mixed with three volumes of PBS, overlaid onto Histopaque-1077 cushions, and centrifuged for 40 min at 400g. PBMCs were collected and washed three times with PBS. PBMCs were then resuspended in RPMI 1640 containing 10% FBS and 1% L-glutamine and counted. The purified PBMCs were then pelleted and resuspended in RNA later before being frozen at -80°C .

For animals infected with nectin-4-blind CDV, whole blood was collected once weekly after infection in Na₂-EDTA tubes for virus titration. Total leukocyte counts were obtained as described above. Blood was centrifuged for 15 min at 3000 rpm, and the plasma was harvested. The remaining cells were mixed with five volumes of red blood cell (RBC) lysis buffer based on the initial volume of blood (~2 ml) and incubated for 10 to 15 min at room temperature. After RBC lysis, the cells were centrifuged and washed once with PBS, and then resuspended in Dulbecco's modified Eagle medium (DMEM) containing 5% FBS and 1% L-glutamine. Titrations were performed by limiting dilution in 96-well plates, and titers were expressed as log₁₀(TCID₅₀/10⁶ PBMCs).

Influenza A/INDRE/Mexico/4487/2009 challenge

Ferrets were infected intranasally with 5×10^5 TCID₅₀ of the virulent 2009 pandemic H1N1 influenza virus strain Mx10 (A/INDRE/Mexico/4487/2009). Nasal washes were performed once daily, and a clinical examination was performed twice daily for the first 4 days after infection and once on day 7. Nasal washes were kept on ice and centrifuged for 1200 rpm for 3 min at 4°C to pellet debris. Nasal wash supernatants were transferred to fresh Eppendorf tubes on ice, titrated by limiting dilution in 96-well plates, and then incubated for 48 hours at 37°C . The medium was then removed from the plates, and influenza-infected cell monolayers were washed once with PBS diluted one-third in water and air-dried at room temperature for 15 min. The plates were heat-fixed at 65°C for 8 hours. Influenza-infected cells were stained with a polyclonal ferret anti-H1N1pdm09 immune serum at a dilution of 1:500 and a goat anti-ferret horse-radish peroxidase (HRP)-conjugated secondary antibody (Bethyl Laboratories) at a dilution of 1:750. Infected cells were visualized by the development of a red precipitate after incubation with 3-amino-9-ethylcarbazole (Sigma) at room temperature.

Determination of neutralizing antibody titers

Ferret plasma samples were diluted in 50 μ l per well of serum-free DMEM in 96-well plates as described above, starting at a dilution of 1:10 and continuing until 1:1280. Plasma dilutions were mixed with 50 μ l per well of serum-free DMEM containing 1×10^2 TCID₅₀ of Mx10. The plasma-virus mixtures were incubated at 37°C for 20 min to allow complexes to form, after which they were added to Madin-Darby canine kidney (MDCK) cells. Neutralization assays were incubated at 37°C for 48 hours and then fixed and stained as described above for nasal wash titrations. The primary antibody to detect infected cells in neutralization assays was a polyclonal ferret anti-H1N1pdm09 immune serum at a dilution of 1:500 in 50 μ l of PBS per well, followed by a goat anti-ferret HRP secondary antibody at a dilution of 1:750.

Determination of clinical score of disease severity after influenza virus challenge

Clinical signs were scored using a 0-1-2-3 scale, with 0 representing the baseline physiological state. The assessed parameters were as follows:

1. temperature ($<38.5^\circ\text{C}/38.5^\circ$ to $39.0^\circ\text{C}/39.0^\circ$ to $39.5^\circ\text{C}/>39.5^\circ\text{C}$),
2. weight loss (none/0 to 5%/5 to 10%/>10% loss of initial weight),

3. activity (normal/calm/depressed/inactive),
4. nasal exudate (none/serous/sero-mucous/muco-purulent),
5. congestion (none/mild/intermediate/severe),
6. sneezing (none/rarely/occasionally/frequently), and
7. assessment of labored breathing (none/occasional wheezing/continuous wheezing/labored breathing).

The scores were added together for each animal at each observation time point to give the clinical score.

SUPPLEMENTARY MATERIALS

immunology.sciencemag.org/cgi/content/full/4/41/eaay6125/DC1

Text. Evaluation of technical accuracy of the obtained BCR repertoires from individuals B35 and B42.

Fig. S1. Example of FACS strategy for stratification of lymphocyte populations.

Fig. S2. Repertoire sampling across time points.

Fig. S3. Changes in clonotype composition of the B naïve compartment.

Table S1. Sampling points and clinical features of measles cohorts (in Excel spreadsheet).

Table S2. FACS-sorted lymphocyte counts and frequencies across sampling points (in Excel spreadsheet).

Table S3. Read processing information and accession numbers for BCR sequencing data (in Excel spreadsheet).

Table S4. Primer sequence information for BCR sequencing (in Excel spreadsheet).

Table S5. Raw data in Excel spreadsheet.

[View/request a protocol for this paper from Bio-protocol.](#)

REFERENCES AND NOTES

1. World Health Organization, Measles; <https://www.who.int/news-room/fact-sheets/detail/measles>.
2. W. J. Moss, D. E. Griffin, Global measles elimination. *Nat. Rev. Microbiol.* **4**, 900–908 (2006).
3. R. D. de Vries, A. W. Mesman, T. B. Geijtenbeek, W. P. Duprex, R. L. de Swart, The pathogenesis of measles. *Curr. Opin. Virol.* **2**, 248–255 (2012).
4. D. E. Griffin, B. J. Ward, E. Jauregui, R. T. Johnson, A. Vaisberg, Immune activation in measles. *N. Engl. J. Med.* **320**, 1667–1672 (1989).
5. M. J. Mina, C. J. Metcalf, R. L. de Swart, A. D. Osterhaus, B. T. Grenfell, Long-term measles-induced immunomodulation increases overall childhood infectious disease mortality. *Science* **348**, 694–699 (2015).
6. K. Gadroen, C. N. Dodd, G. M. C. Masclee, M. A. J. de Ridder, D. Weibel, M. J. Mina, B. T. Grenfell, M. C. J. M. Sturkenboom, D. A. M. C. van de Vijver, R. L. de Swart, Impact and longevity of measles-associated immune suppression: A matched cohort study using data from the THIN general practice database in the UK. *BMJ Open* **8**, e021465 (2018).
7. D. E. Griffin, T. R. Moench, R. T. Johnson, I. Lindo de Soriano, A. Vaisberg, Peripheral blood mononuclear cells during natural measles virus infection: Cell surface phenotypes and evidence for activation. *Clin. Immunol. Immunopathol.* **40**, 305–312 (1986).
8. T. Vuorinen, P. Peri, R. Vainionpää, Measles virus induces apoptosis in uninfected bystander T cells and leads to granzyme B and caspase activation in peripheral blood mononuclear cell cultures. *Eur. J. Clin. Invest.* **33**, 434–442 (2003).
9. B. Zweiman, In vitro effects of measles virus on proliferating human lymphocytes. *J. Immunol.* **106**, 1154–1158 (1971).
10. P. Casali, G. P. Rice, M. B. Oldstone, Viruses disrupt functions of human lymphocytes. Effects of measles virus and influenza virus on lymphocyte-mediated killing and antibody production. *J. Exp. Med.* **159**, 1322–1337 (1984).
11. B. J. Ward, R. T. Johnson, A. Vaisberg, E. Jauregui, D. E. Griffin, Cytokine production in vitro and the lymphoproliferative defect of natural measles virus infection. *Clin. Immunol. Immunopathol.* **61**, 236–248 (1991).
12. R. D. de Vries, R. L. de Swart, Measles immune suppression: Functional impairment or numbers game? *PLOS Pathog.* **10**, e1004482 (2014).
13. R. D. de Vries, S. McQuaid, G. van Amerongen, S. Yüksel, R. J. Verburgh, A. D. M. E. Osterhaus, W. P. Duprex, R. L. de Swart, Measles immune suppression: Lessons from the macaque model. *PLOS Pathog.* **8**, e1002885 (2012).
14. H. Tatsuo, N. Ono, K. Tanaka, Y. Yanagi, SLAM (CDw150) is a cellular receptor for measles virus. *Nature* **406**, 893–897 (2000).
15. R. L. de Swart, M. Ludlow, L. de Witte, Y. Yanagi, G. van Amerongen, S. McQuaid, S. Yüksel, T. B. H. Geijtenbeek, W. P. Duprex, A. D. M. E. Osterhaus, Predominant infection of CD150+ lymphocytes and dendritic cells during measles virus infection of macaques. *PLOS Pathog.* **3**, e178 (2007).
16. A. N. Nelson, N. Putnam, D. Hauer, V. K. Baxter, R. J. Adams, D. E. Griffin, Evolution of T cell responses during measles virus infection and RNA clearance. *Sci. Rep.* **7**, 11474 (2017).
17. B. M. Laksono, R. D. de Vries, R. J. Verburgh, E. G. Visser, A. de Jong, P. L. A. Fraaij, W. L. M. Ruijs, D. F. Nieuwenhuijse, H.-J. van den Ham, M. P. G. Koopmans, M. C. van Zelm, A. D. M. E. Osterhaus, R. L. de Swart, Studies into the mechanism of measles-associated immune suppression during a measles outbreak in the Netherlands. *Nat. Commun.* **9**, 4944 (2018).
18. F. M. Burnet, A modification of Jerne's theory of antibody production using the concept of clonal selection. *CA Cancer J. Clin.* **26**, 119–121 (1976).
19. N. Jiang, J. He, J. A. Weinstein, L. Penland, S. Sasaki, X. S. He, C. L. Dekker, N.-Y. Zheng, M. Huang, M. Sullivan, P. C. Wilson, H. B. Greenberg, M. M. Davis, D. S. Fisher, S. R. Quake, Lineage structure of the human antibody repertoire in response to influenza vaccination. *Sci. Transl. Med.* **5**, 171ra119 (2013).
20. V. N. Petrova, L. Muir, P. F. McKay, G. S. Vassiliou, K. G. C. Smith, P. A. Lyons, C. A. Russell, C. A. Anderson, P. Kellam, R. J. M. Bashford-Rogers, Combined influence of B-cell receptor rearrangement and somatic hypermutation on B-cell class-switch fate in health and in chronic lymphocytic leukemia. *Front. Immunol.* **9**, 1784 (2018).
21. M. S. Cabatingan, M. R. Schmidt, R. Sen, R. T. Woodland, Naive B lymphocytes undergo homeostatic proliferation in response to B cell deficit. *J. Immunol.* **169**, 6795–6805 (2002).
22. C. F. A. de Bourcy, C. L. Dekker, M. M. Davis, M. R. Nicolls, S. R. Quake, Dynamics of the human antibody repertoire after B cell depletion in systemic sclerosis. *Sci. Immunol.* **2**, eaan8289 (2017).
23. R. J. Bashford-Rogers, A. L. Palsler, B. J. Huntly, R. Rance, G. S. Vassiliou, G. A. Follows, P. Kellam, Network properties derived from deep sequencing of human B-cell receptor repertoires delineate B-cell populations. *Genome Res.* **23**, 1874–1884 (2013).
24. J. L. Wynn, O. Levy, Role of innate host defenses in susceptibility to early-onset neonatal sepsis. *Clin. Perinatol.* **37**, 307–337 (2010).
25. M. M. Souto-Carneiro, G. P. Sims, H. Girschik, J. Lee, P. E. Lipsky, Developmental changes in the human heavy chain CDR3. *J. Immunol.* **175**, 7425–7436 (2005).
26. E. Rechavi, A. Lev, Y. N. Lee, A. J. Simon, Y. Yinon, S. Lipitz, N. Amariglio, B. Weisz, L. D. Notarangelo, R. Somech, Timely and spatially regulated maturation of B and T cell repertoire during human fetal development. *Sci. Transl. Med.* **7**, 276ra225 (2015).
27. J. E. Berman, K. G. Nickerson, R. R. Pollock, J. E. Barth, R. K. B. Schuurman, D. M. Knowles, L. Chess, F. W. Alt, V_H gene usage in humans: Biased usage of the V_H6 gene in immature B lymphoid cells. *Eur. J. Immunol.* **21**, 1311–1314 (1991).
28. B. M. Laksono, C. Grosserichter-Wagener, R. D. de Vries, S. A. G. Langeveld, M. D. Brem, J. J. M. van Dongen, P. D. Katsikis, M. P. G. Koopmans, M. C. van Zelm, R. L. de Swart, In vitro measles virus infection of human lymphocyte subsets demonstrates high susceptibility and permissiveness of both naive and memory B cells. *J. Virol.* **92**, e00131-e18 (2018).
29. C. A. Janeway Jr., P. Travers, M. Walport, M. J. Shlomchik, The distribution and functions of immunoglobulin isotypes, in *Immunobiology: The Immune System in Health and Disease* (Garland Science, ed. 5, 2001).
30. P. Roll, A. Palanichamy, C. Kneitz, T. Dörner, H.-P. Tony, Regeneration of B cell subsets after transient B cell depletion using anti-CD20 antibodies in rheumatoid arthritis. *Arthritis Rheum.* **54**, 2377–2386 (2006).
31. K. Muhammad, P. Roll, H. Einsele, T. Dörner, H. P. Tony, Delayed acquisition of somatic hypermutations in repopulated IGD+CD27+ memory B cell receptors after rituximab treatment. *Arthritis Rheum.* **60**, 2284–2293 (2009).
32. A. Hu, H. Sheshberadaran, E. Norrby, J. Kóvamees, Molecular characterization of epitopes on the measles virus hemagglutinin protein. *Virology* **192**, 351–354 (1993).
33. V. von Messling, C. Springfield, P. Devaux, R. Cattaneo, A ferret model of canine distemper virus virulence and immunosuppression. *J. Virol.* **77**, 12579–12591 (2003).
34. B. Sawatsky, X.-X. Wong, S. Hinkelmann, R. Cattaneo, V. von Messling, Canine distemper virus epithelial cell infection is required for clinical disease but not for immunosuppression. *J. Virol.* **86**, 3658–3666 (2012).
35. T. C. Nessler, B. Scallon, Chimeric antibodies with extended half-life in ferrets. *Influenza Other Respir. Viruses* **8**, 596–604 (2014).
36. D. L. Miller, Frequency of complications of measles, 1963. Report on a national inquiry by the public health laboratory service in collaboration with the society of medical officers of health. *Br. Med. J.* **2**, 75–78 (1964).
37. A. P. Beckford, R. O. Kaschula, C. Stephen, Factors associated with fatal cases of measles. A retrospective autopsy study A retrospective autopsy study. *S. Afr. Med. J.* **68**, 858–863 (1985).
38. M. B. McChesney, J. H. Kehrl, A. Valsamakis, A. S. Fauci, M. B. Oldstone, Measles virus infection of B lymphocytes permits cellular activation but blocks progression through the cell cycle. *J. Virol.* **61**, 3441–3447 (1987).
39. M. B. McChesney, R. S. Fujinami, P. W. Lampert, M. B. Oldstone, Viruses disrupt functions of human lymphocytes. II. Measles virus suppresses antibody production by acting on B lymphocytes. *J. Exp. Med.* **163**, 1331–1336 (1986).
40. R. T. Woodland, M. R. Schmidt, Homeostatic proliferation of B cells. *Semin. Immunol.* **17**, 209–217 (2005).

41. I. Boussaad, L. Varagnolo, V. Hornich, L. Rieger, M. Krockenberger, T. Stuehmer, D. Kranzfelder, A. M. Mueller, S. Schneider-Schaulies, Wild-type measles virus interferes with short-term engraftment of human CD34⁺ hematopoietic progenitor cells. *J. Virol.* **85**, 7710–7718 (2011).
42. R. T. Perry, N. A. Halsey, The clinical significance of measles: A review. *J. Infect. Dis.* **189** Suppl 1, S4–S16 (2004).
43. R. M. D'Souza, R. D'Souza, Vitamin A for treating measles in children. *Cochrane Database Syst. Rev.*, CD001479 (2002).
44. N. Cabezas-Wallscheid, F. Buettner, P. Sommerkamp, D. Klimmeck, L. Ladel, F. B. Thalheimer, D. Pastor-Flores, L. P. Roma, S. Renders, P. Zeisberger, A. Przybylla, K. Schönberger, R. Scognamiglio, S. Altamura, C. M. Florian, M. Fawaz, D. Vonficht, M. Tesio, P. Collier, D. Pavlinic, H. Geiger, T. Schroeder, V. Benes, T. P. Dick, M. A. Rieger, O. Stegle, A. Trumpp, Vitamin A-retinoic acid signaling regulates hematopoietic stem cell dormancy. *Cell* **169**, 807–823.e19 (2017).
45. K. Rajewsky, Clonal selection and learning in the antibody system. *Nature* **381**, 751–758 (1996).
46. A. D. Gitlin, L. von Boehmer, A. Gazumyan, Z. Shulman, T. Y. Oliveira, M. C. Nussenzweig, Independent roles of switching and hypermutation in the development and persistence of B lymphocyte memory. *Immunity* **44**, 769–781 (2016).
47. N. L. Bernasconi, E. Traggiai, A. Lanzavecchia, Maintenance of serological memory by polyclonal activation of human memory B cells. *Science* **298**, 2199–2202 (2002).
48. J. H. Anolik, J. Barnard, T. Owen, B. Zheng, S. Kemshtetti, R. J. Looney, I. Sanz, Delayed memory B cell recovery in peripheral blood and lymphoid tissue in systemic lupus erythematosus after B cell depletion therapy. *Arthritis Rheum.* **56**, 3044–3056 (2007).
49. D. Bedognetti, G. Zoppoli, C. Massucco, E. Zanardi, S. Zupo, A. Bruzzone, M. R. Sertoli, E. Balleari, O. Racchi, M. Messina, G. Caltabiano, G. Icardi, P. Durando, F. M. Marincola, F. Boccardo, M. Ferrarini, F. Ansaldo, A. de Maria, Impaired response to influenza vaccine associated with persistent memory B cell depletion in non-Hodgkin's lymphoma patients treated with rituximab-containing regimens. *J. Immunol.* **186**, 6044–6055 (2011).
50. O. E. Yri, D. Torfoss, O. Hungnes, A. Tierens, K. Waalen, T. Nordøy, S. Dudman, A. Kilander, K. F. Wader, B. Østenstad, R. Ekanger, P. Meyer, A. Kolstad, Rituximab blocks protective serologic response to influenza A (H1N1) 2009 vaccination in lymphoma patients during or within 6 months after treatment. *Blood* **118**, 6769–6771 (2011).
51. J. Westra, S. van Assen, K. R. Wilting, J. Land, G. Horst, A. de Haan, M. Bijl, Rituximab impairs immunoglobulin (Ig)M and IgG (subclass) responses after influenza vaccination in rheumatoid arthritis patients. *Clin. Exp. Immunol.* **178**, 40–47 (2014).
52. E. Alamyar, P. Duroux, M. P. Lefranc, V. Giudicelli, IMGT® tools for the nucleotide analysis of immunoglobulin (IG) and T cell receptor (TR) V-(D)-J repertoires, polymorphisms, and IG mutations: IMGT/V-QUEST and IMGT/HighV-QUEST for NGS. *Methods Mol. Biol.* **882**, 569–604 (2012).
53. M. Shugay, D. V. Bagaev, M. A. Turchaninova, D. A. Bolotin, O. V. Britanova, E. V. Putintseva, M. V. Pogorelyy, V. I. Nazarov, I. V. Zvyagin, V. I. Kirgizova, K. I. Kirgizov, E. V. Skorobogatova, D. M. Chudakov, VDJtools: Unifying post-analysis of T cell receptor repertoires. *PLoS Comput. Biol.* **11**, e1004503 (2015).
54. I. Meunier, C. Embury-Hyatt, S. Stebner, M. Gray, N. Bastien, Y. Li, F. Plummer, G. P. Kobinger, V. von Messling, Virulence differences of closely related pandemic 2009 H1N1 isolates correlate with increased inflammatory responses in ferrets. *Virology* **422**, 125–131 (2012).

Acknowledgments: We thank Y. Krebs for assistance with the ferret antibody assays and L. Walbridge and J. Baxter from the Cambridge Blood and Stem Cell Biobank for providing the CLL sample. **Funding:** B.M.L. was supported by the Indonesian Endowment Fund for Education (LPDP). V.N.P. and C.A.A. were supported by a grant from the Wellcome Trust (206194), which also funded all the sequencing. V.v.M. and B.S. were supported by funding from the German Centre for Infection Research (DZIF-TTU Emerging Infections), the Collaborative Research Centre (SFB 1021) of the German Research Foundation (DFG), and the German Ministry of Health. C.A.R. was supported by a University Research Fellowship from the Royal Society. **Author contributions:** V.N.P., P.K., V.v.M., R.L.d.S., and C.A.R. conceived and designed the research. R.D.d.V. and R.L.d.S. coordinated the collection of the clinical specimens. B.S., L.W., and V.v.M. performed the ferret experiments. V.N.P. performed the BCR sequencing and data analyses and created the figures along with A.X.H., C.A.A., and C.A.R. V.N.P. and C.A.R. drafted the manuscript with substantial support from B.M.L., R.D.d.V., and R.L.d.S. All authors discussed the results and contributed to the revision of the final manuscript. **Competing interests:** The authors declare they have no competing interests. **Data and materials availability:** All of the code developed for the data analyses is available through a project-specific GitHub repository (<https://github.com/VelislavaNPetrova/measlespaper/>). The IGH sequences were deposited in the European Genome-Phenome Archive (EGA) under study accession number EGAS00001002635 as dataset EGAD00001003749. Individual accession numbers are provided in table S3. Because the immunoglobulin sequences constitute human data, they are stored under managed data access according to the Wellcome Sanger Institute data release policy. Access to these samples must be requested from the Data Access Committee (DAC), whose contact details can be found on the EGA study page, accessible through the study accession numbers or by emailing datasharing@sanger.ac.uk. The requester will be required to sign a data access agreement, which is in place to protect the identity of the sample donors via a managed access system. All other data needed to evaluate the conclusions in the paper are present in the paper and/or the Supplementary Materials.

Submitted 3 July 2019

Accepted 1 October 2019

Published 1 November 2019

10.1126/sciimmunol.aay6125

Citation: V. N. Petrova, B. Sawatsky, A. X. Han, B. M. Laksono, L. Walz, E. Parker, K. Pieper, C. A. Anderson, R. D. de Vries, A. Lanzavecchia, P. Kellam, V. von Messling, R. L. de Swart, C. A. Russell, Incomplete genetic reconstitution of B cell pools contributes to prolonged immunosuppression after measles. *Sci. Immunol.* **4**, eaay6125 (2019).

Incomplete genetic reconstitution of B cell pools contributes to prolonged immunosuppression after measles

Velislava N. Petrova, Bevan Sawatsky, Alvin X. Han, Brigitta M. Laksono, Lisa Walz, Edyth Parker, Kathrin Pieper, Carl A. Anderson, Rory D. de Vries, Antonio Lanzavecchia, Paul Kellam, Veronika von Messling, Rik L. de Swart and Colin A. Russell

Sci. Immunol. 4, eaay6125.
DOI: 10.1126/sciimmunol.aay6125

Measles infection prunes back B cell memory

Measles virus is a highly infectious lymphotropic virus associated with an extended period of immunosuppression after resolution of acute viremia. Petrova *et al.* sequenced the immunoglobulin gene repertoire of naïve and memory B cells in paired pre- and post-measles infection blood samples from unvaccinated children. Memory B cell clones present before infection were depleted in post-measles samples even after lymphocyte counts had recovered, a change not seen in controls given a flu vaccination. The naïve B cell repertoire exhibited multiple perturbations after measles infection, including a profound skew toward clones with immature features in ~10% of the cohort. The B cell repertoire changes documented in this study provide a molecular explanation for the durable "immune amnesia" observed after measles infection in unvaccinated populations.

ARTICLE TOOLS

<http://immunology.sciencemag.org/content/4/41/eaay6125>

SUPPLEMENTARY MATERIALS

<http://immunology.sciencemag.org/content/suppl/2019/10/25/4.41.eaay6125.DC1>

REFERENCES

This article cites 51 articles, 17 of which you can access for free
<http://immunology.sciencemag.org/content/4/41/eaay6125#BIBL>

PERMISSIONS

<http://www.sciencemag.org/help/reprints-and-permissions>

Use of this article is subject to the [Terms of Service](#)